ISSN 1674-1056
http://cpb.iphy.ac.cn
http://iopscience.iop.org/cpb
中国物理 B
Chinese Physics
中国物理 Chinese Physics B

Room-temperature continuous-wave interband cascade laser emitting at 3.45 μm

Yi Zhang(张一), Fu-Hui Shao(邵福会), Cheng-Ao Yang(杨成奥), Sheng-Wen Xie(谢圣文), Shu-Shan Huang(黄书山), Ye Yuan(袁野), Jin-Ming Shang(尚金铭), Yu Zhang(张宇), Ying-Qiang Xu(徐应强), Hai-Qiao Ni(倪海桥), Zhi-Chuan Niu(牛智川)

Citation: Chin. Phys. B . 2018, 27(12): 124207. **doi:** 10.1088/1674-1056/27/12/124207
Journal homepage: http://cpb.iphy.ac.cn; http://iopscience.iop.org/cpb

What follows is a list of articles you may be interested in

Double-rod metasurface for mid-infrared polarization conversion

Yang Pu(蒲洋), Yi Luo(罗意), Lu Liu(刘路), De He(何德), Hongyan Xu(徐洪艳), Hongwei Jing(景洪伟), Yadong Jiang(蒋亚东), Zhijun Liu(刘志军)

Chin. Phys. B . 2018, 27(2): 024202. **doi:** 10.1088/1674-1056/27/2/024202

Self-compression of 1.8-μm pulses in gas-filled hollow-core fibers

Rui-Rui Zhao(赵睿睿), Ding Wang(王丁), Yu Zhao(赵钰), Yu-Xin Leng(冷雨欣), Ru-Xin Li(李儒新)

Chin. Phys. B . 2017, 26(10): 104206. **doi:** 10.1088/1674-1056/26/10/104206

Broadband tunable Raman soliton self-frequency shift to mid-infrared band in a highly birefringent microstructure fiber

Wei Wang(王伟), Xin-Ying Bi(毕新英), Jun-Qi Wang(王珺琪), Yu-Wei Qu(屈玉玮), Ying Han(韩颖), Gui-Yao Zhou(周桂耀), Yue-Feng Qi(齐跃峰)

Chin. Phys. B . 2016, 25(7): 074206. **doi:** 10.1088/1674-1056/25/7/074206

Optimization of the idler wavelength tunable cascaded optical parametric oscillator based on chirp-assisted aperiodically poled lithium niobate crystal

Tao Chen(陈滔), Rong Shu(舒嵘), Ye Ge(葛烨), Zhuo Chen(陈卓)

Chin. Phys. B . 2016, 25(1): 014209. **doi:** 10.1088/1674-1056/25/1/014209

Spectroscopic properties of heavily Ho^{3+}-doped barium yttrium fluoride crystals

Ji En-Cai, Liu Qiang, Nie Ming-Ming, Luo Hui, Hu Yu-Xi, Guan Zhou-Guo, Gong Ma-Li

Chin. Phys. B . 2015, 24(9): 094216. **doi:** 10.1088/1674-1056/24/9/094216

Room-temperature continuous-wave interband cascade laser emitting at 3.45 μm*

Yi Zhang(张一)[1,2,3], Fu-Hui Shao(邵福会)[1,2,3], Cheng-Ao Yang(杨成奥)[1,2,3], Sheng-Wen Xie(谢圣文)[1,2,3], Shu-Shan Huang(黄书山)[1,2,3], Ye Yuan(袁野)[1,2,3], Jin-Ming Shang(尚金铭)[1,2,3], Yu Zhang(张宇)[1,2,3,†], Ying-Qiang Xu(徐应强)[1,2,3], Hai-Qiao Ni(倪海桥)[1,2,3], and Zhi-Chuan Niu(牛智川)[1,2,3,‡]

[1] *State Key Laboratory for Superlattices and Microstructures, Institute of Semiconductor, Chinese Academy of Sciences, Beijing* 100083 *China*

[2] *College of Materials Science and Opto-Electronic Technology, University of Chinese Academy of Sciences, Beijing* 101408, *China*

[3] *Synergetic Innovation Center of Quantum Information and Quantum Physics, University of Science and Technology of China, Hefei* 230026, *China*

(Received 14 August 2018; revised manuscript received 1 September 2018; published online 25 November 2018)

We report a type-II GaSb-based interband cascade laser operating a continuous wave at room temperature. The cascade region of interband cascade laser was designed using the 'W' configuration of the active quantum wells and the 'Carrier Rebalancing' method in the electron injector. The devices were processed into narrow ridges and mounted epitaxial side down on a copper heat sink. The 25-μm-wide, 3-mm-long ridge without coated facets generated 41.4 mW of continuous wave output power at $T = 15$ °C. And a low threshold current density of 267 A/cm^2 is achieved. The emission wavelength of the ICL is 3452.3 nm at 0.5 A.

Keywords: interband cascade laser, mid-infrared, GaSb-based, type-II W quantum well

PACS: 42.55.Px, 78.55.Cr, 78.67.Pt, 42.60.Pk **DOI:** 10.1088/1674-1056/27/12/124207

1. Introduction

The mid-infrared (defined here as 3 μm–4 μm) spectral region is getting more and more attention, because it includes many 'fingerprint' spectral lines of gases such as methane, carbon dioxide, carbon monoxide formaldehyde, *etc*. At present, there are three kinds of lasers that can realize 3 μm–4 μm spectral region including type-I quantum well laser (and type-I quantum well cascade laser),[1–5] quantum cascade laser (QCL),[6,7] and interband cascade laser (ICL).[8,9] However, the type-I quantum well laser and type-I quantum well cascade laser are limited by the Auger non-radiative decay and the carriers escape associated with insufficient valence-band offset under 3 μm–4 μm. Besides, the quantum cascade laser (QCL) is suffered from the rapid phonon-assisted scattering and the insufficient conduction-band offset which result in QCL's high threshold current density. The interband cascade laser can make up for these shortcomings and cover the whole 3 μm–4 μm spectral region.

The interband cascade laser is a promising 3 μm–4 μm source which can be used in medical devices, industrial gas detection[10] and free-space optical communications. For the traditional diode laser, the carrier injection is realized by parallel in the multi quantum wells (MQWs). However, in the cascade laser (ICL and QCL), the active regions are in series.[11] Ideally, the number of photons produced by an electron is determined by the cascade number N, which results in the quantum efficiency of the cascade structure being greater than 100%. At the same time, the working current of cascade laser is N times smaller than the traditional parallel diode laser, but the corresponding voltage will increase substantially. The result of trading a higher threshold voltage for a lower threshold current is that the power consumption from the parasitic resistance is N^2 times smaller than traditional parallel diode laser. This leads to higher quantum efficiency and lower threshold current for interband cascade laser.[12] Although both the interband cascade laser and quantum cascade lasers have cascade structures, the quantum cascade lasers are unipolar devices, and the transport and recombination processes of the electrons occur in conduction band which cannot avoid the participation of the rapid phonon-assisted scattering. However, the interband cascade laser is based on the type-II interband transition, and the recombination is complete in the electrons in the conduction band and the holes in the valence band. Because of the two opposite dispersion curves of conduction band and valence band, the electron interband transition does not allow the participation of the rapid phonon-assisted scattering. This makes it unnecessary for a interband cascade laser to achieve population inversion by means of rapid phonon-

*Project supported by the Major Program of the National Natural Science Foundation of China (Grant No. 61790580), the National Natural Science Foundation of China (Grant No. 61435012), and the National Basic Research Program of China (Grant No. 2014CB643903).

†Corresponding author. E-mail: zhangyu@semi.ac.cn

‡Corresponding author. E-mail: zcniu@semi.ac.cn

© 2018 Chinese Physical Society and IOP Publishing Ltd

assisted scattering and multi-level as quantum cascade laser. Therefore, the threshold current, voltage and power consumption can be significantly reduced in the interband cascade laser than QCL.[13]

Another difference between interband cascade lasers and conventional quantum well lasers is that the interband cascade lasers use type-II interband transitions. For traditional type-I quantum well laser, the wave function of the electron and hole is confined in the same layer and its transition is a kind of direct transition. However, for the interband cascade lasers, the combination of the electrons and holes is not in the same layer, and the wave functions of the electrons and holes are also distributed in different layers. In interband cascade laser, the luminescence wavelength is not determined by the band gap $E_g = E_c - E_v$, but by the electrons and holes in the different layers of two quantum well for which the $E_g = E_e - E_h$.[14]

At present, there are only a few research units in the world which can achieve the interband cascade lasers including the University of Oklahoma, the Naval Research Laboratory (NRL), the Wurzburg University, and our group of the semiconductor in Institute of Semiconductor, the Chinese Academy of Sciences, reported in this work. In 2008, the Naval Research Laboratory (NRL) first realized the continuous operation of interband cascade laser at room temperature.[9] And after further optimization, in 2014 the NRL has achieved continuous-wave 592-mW output power at room temperature.[15] And the lowest threshold current density of interband cascade laser has been as low as 98 A/cm^2.[13] However, there is no report of interband cascade laser operating at room temperature in China.

In this paper, we present a process of fabricating interband cascade laser operating at room temperature in continuous wave. We will start from the growth of materials, especially the structure and design of cascade region, such as the rebalancing of carries and the type-II 'W' configuration of the active quantum wells. On the basis of this, we will fabricate the full structure of interband cascade laser and then characterize the growth of the materials. Finally, we will introduce the fabrication process of the devices and analyze the result of ICL in this work.

2. Material structure and characterization

The interband cascade lasers in this work were grown on Te-doped n-GaSb substrates by a Gen-II molecular beam epitaxy machine with solid sources for the group-III elements and valved cracker cells for both arsenic and antimony. And the Si and Te crackers were used for doping. The growth temperature was ramped down for epitaxial growth after thermal oxide desorption under Sb_2 stabilization at 560 °C for 15 min.[16] Subsequently, the growth was initiated with a 300-nm thick Te-doped (1×10^{18} cm^{-3}) GaSb buffer layer for a better surface and Ohmic contact. This buffer was followed by a thick superlattice (SL) lower cladding. The lower cladding comprised InAs/AlSb superlattice with a period of 4.73 nm which was lattice-matched to GaSb substrate. Then a Te-doped GaSb separate-confinement layer (SCL) was grown. The GaSb SCL was used to concentrate the optical mode in the active region because of the high refractive index of the GaSb layer.[17] After the SCL growth, it came to the cascade region. The cascade region comprised 5 active stages published in Ref. [12]. The layer structure of one period of active region was as follows: 2.5-nm AlSb/1.7-nm InAs/3.0-nm $In_{0.35}Ga_{0.65}Sb$/1.4-nm InAs/1.0-nm AlSb/3.0-nm GaSb/1.0-nm AlSb/4.5-nm GaSb/2.5-nm AlSb/4.2-nm InAs/1.2-nm AlSb/3.2-nm InAs/1.2-nm AlSb/2.5-nm InAs/1.2-nm AlSb/2.0-nm InAs/1.2-nm AlSb/1.7-nm InAs/1.2-nm AlSb/1.7-nm InAs.[18]

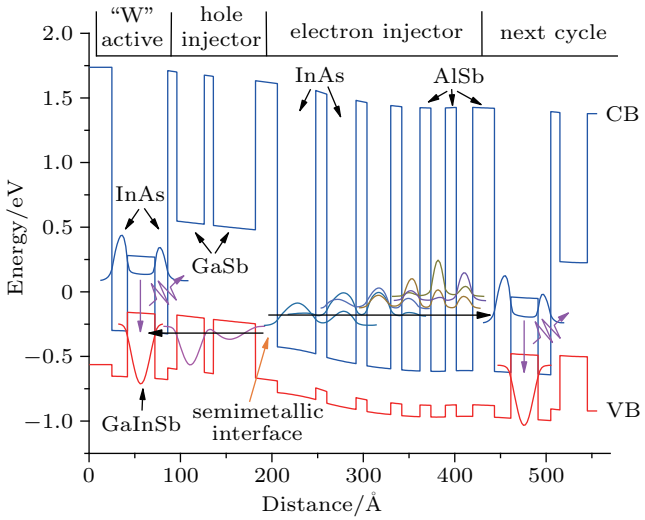


Fig. 1. (color online) The band structure of the cascade region of ICL.

As shown in Fig. 1, one period of active stage consisted of the 'W' active region, the hole injector, and the electron injector.[19] The advantage of using the 'W' configuration of the active quantum wells is to enhance the electron–hole wavefunction overlap in comparison to that for an InAs/InGaSb QW with a single type-II interface.[20] Besides, the four InAs layers in the electron injector were heavily n-type doped with Si to 5×10^{18} cm^{-3} so that the internally generated carriers were rebalanced. It has been reported that the 'Carrier Rebalancing' in the ICL provided better performance for the 'W' active region with regard to lowest threshold current densities and turn-on voltages.[21] Right after the cascade region, the top SCL was grown in a symmetrical fashion. Then, a less thick top cladding (a period of 4.73-nm InAs/AlSb superlattices) was grown. The interband cascade laser was finalized with a heavily Si-doped (5×10^{18} cm^{-3}) InAs contact layer,

which was about 20 nm to reduce the contact resistance. In addition, the transition layers were inserted in the boundary of different regions to minimize the parasitic voltages drops. The device is schematically shown in Fig. 2.

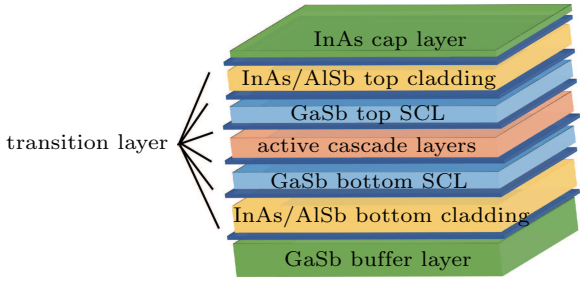


Fig. 2. (color online) The full structure of the interband cascade laser.

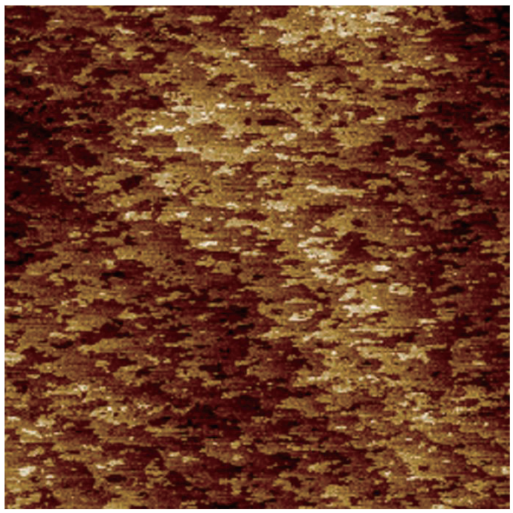


Fig. 3. 10 μm×10 μm AFM scan of the interband cascade laser.

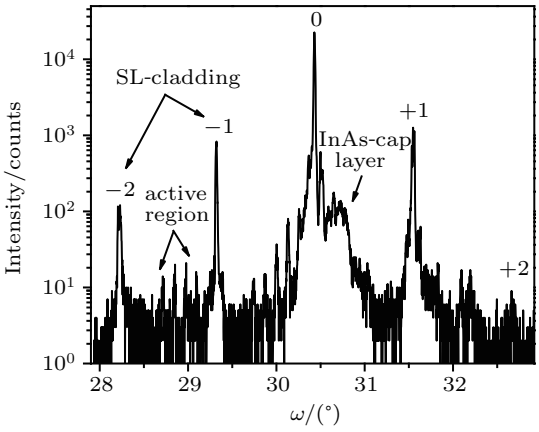


Fig. 4. The HRXRD spectrum of the 5 stages ICL ([004] reflection). The InAs/AlSb superlattices in the picture respond to the sharp peaks. The small peaks correspond to active cascade region. And the wider peak to the right of the center peaks arises from the 20 nm-thick InAs cap layer.

The high-resoltion x-ray diffraction (HRXRD) and atomic force microscopy (AFM) were used to characterize the growth quality of the material. Figure 3 shows the AFM image of a 10 μm×10 μm size of the interband cascade laser. The long atomic steps on the surface with a root mean square (RMS) surface roughness of 1.33 Å show the excellent material growth quality. The HRXRD curve is shown in Fig. 4. The central peak for the InAs/AlSb superlattices cladding layers is nearly coincident with the GaSb substrate peak indicating the lattice-matched growth.

3. Laser performance

Using standard contact lithography in combination with inductively coupled plasma (ICP) etching techniques, the 25-μm-wide narrow ridges were fabricated. To prevent current diffusion, the etch had to stop in the bottom GaSb SCL. After the dry etch, the clean-up phosphoric-acid-based wet etch is followed to minimize the damage to the side wall. A 250-nm thick SiO_2 insulation layer was deposited using plasma enhanced chemical vapor deposition (PECVD) and a 15-μm-wide injection window was opened with dry-etching. Then 50/50/1000-nm Ti/Pt/Au was sputtered as the contact electrode. Following substrate mechanical thinning and chemical mechanical polishing, the bottom Ohmic contacts are achieved by metallization and annealing.

All devices are mounted epi-side down on a copper heatsink. The FTIR (Fourier-transform infrared) method is used to measure the emission spectra. Figure 5 shows the emission spectra of the interband cascade laser with a current of 0.5 A. The emission wavelength of the interband cascade laser is 3452.3 nm at 0.5 A. The full width at half maximum (FWHM) of the interband cascade laser is about 52 nm which shows that the emission spectrum is comprised of multiple longitudinal modes and the existence of higher-order optical modes exists in the 25-μm-wide narrow ridges. The lasing wavelength is relatively stable and does not change over a long period of time under the temperature control platform at $T = 15$ °C.

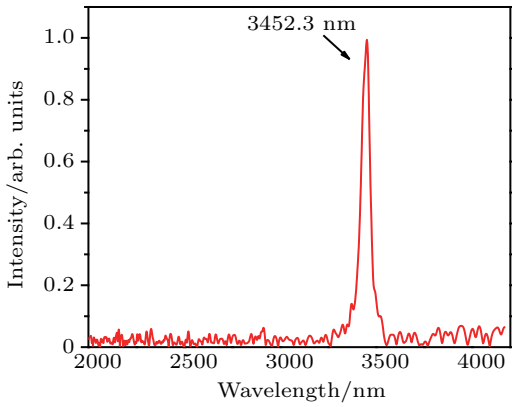


Fig. 5. (color online) The light-current–voltage characteristics of the interband cascade lasers at room temperature in continuous wave.

A calibrated thermopile detector and current source are used to measure the output characteristics. The 25-μm-wide, 3-mm-long devices without HR/AR coated facets are measured. Figure 6 shows the light-current–voltage characteristics of the interband cascade lasers at room temperature in continuous wave (CW) regime. The 25-μm wide ridge devices

without coated facets show a low threshold current density of 267 A/cm^2 and the lasers emit more than 41 mW of optical power with a current of 0.6 A. Thus the differential quantum efficiency is estimated to be 113.8 mW/A. In addition, we find that when the current is greater than 0.5 A, the slope efficiency of the device has decreased due to the thermal accumulation effect. The degradation of the devices occurs when the current is added to more than 0.6 A. The maximum output power of 0.6 A is limited by thermal rollover. The turn-on voltage is 3.8 V and the operation voltage increases rapidly as the current increases which is mainly caused by the large series resistance. The parasitic voltage drop is about 2.5 V and a "voltage efficiency" is about 35%. The high parasitic voltage drop and low voltage efficiency indicate that the series resistance is very large compared to the result of NRL (voltage efficiency $>$ 67%). At maximum current, the differential series resistance tested at room temperature is 3.6 mΩ·cm^2 while the differential series resistance is only 0.5 mΩ·cm^2 of NRL.[17] This can be improved by optimizing the material growth especially the interface of different layers and the growth quality of cladding layers.

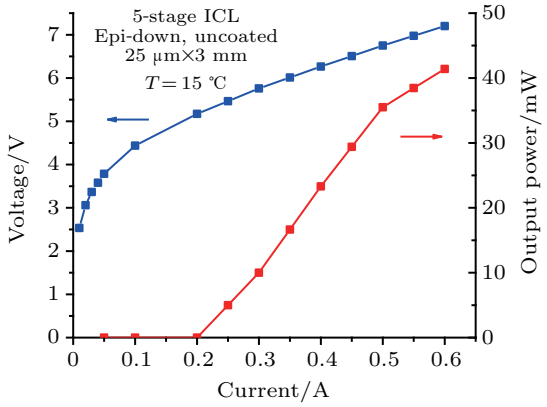


Fig. 6. (color online) The light-current–voltage characteristics of the 5-stage 25 μm×3 mm interband cascade lasers at room temperature in continuous wave.

4. Conclusion and perspectives

In summary, we successfully grew the interband cascade lasers by using optimal growth parameters. The cascade region of interband cascade laser was designed according to the 'W' configuration of active region and the 'rebalancing of the carriers'. The full structure of ICL includes lattice matched superlattice cladding layers, GaSb SCLs, and cascade region. The ICL was fabricated in a standard process. The 25-μm-wide, 3-mm-long narrow-ridge devices (uncoated) emit up to 41.4 mW at room temperature in continuous wave. The threshold current of ICL is about 267 A/cm^2 and its emission wavelength is about 3.45 μm. Room-temperature continuous-wave interband cascade laser has been realized. We believe that we can get better device performance after further optimization.

References

[1] Grau M, Lin C, Dier O, Lauer C and Amann M C 2005 *Appl. Phys. Lett.* **87** 241104
[2] Shterengas L, Belenky G, Kipshidze G and Hosoda T 2008 *Appl. Phys. Lett.* **92** 171111
[3] Shterengas L, Liang R, Kipshidze G, Hosoda T, Suchalkin S and Belenky G 2013 *Appl. Phys. Lett.* **103** 121108
[4] Shterengas L, Liang R, Kipshidze G and Hosoda T 2014 *Appl. Phys. Lett.* **105** 161112
[5] Hosoda T, Wang M, Shterengas L, Kipshidze G and Belenky G 2015 *Appl. Phys. Lett.* **107** 111106
[6] Bandyopadhyay N, Bai Y, Tsao S, Nida S, Slivken S and Razeghi M 2012 *Appl. Phys. Lett.* **101** 241110
[7] Bandyopadhyay N, Slivken S, Bai Y and Razeghi M 2012 *Appl. Phys. Lett.* **100** 212104
[8] Canedy C L, Bewley W W, Lindle J R, Kim C S, Kim M, Vurgaftman I and Meyer J R 2006 *Appl. Phys. Lett.* **88** 161103
[9] Kim M, Canedy C L, Bewley W W, Kim C S, Lindle J R, Abell J, Vurgaftman I and Meyer J R 2008 *Appl. Phys. Lett.* **92** 191110
[10] Garimard Q, Nguyenba T, Larrue A, Cerutti L, Rouillard Y, Gauthier O, Teissier R and Vicet A 2014 *Proc. SPIE* **9134** 91341J
[11] Vurgaftman I, Bewley W W, Merritt C D, Canedy C L, Kim C S, Abell J, Meyer J R and Kim M 2012 *Proc. SPIE* **8268** 82681F
[12] Bewley W W, Merritt C D, Kim C S, Kim M, Canedy C L, Vurgaftman I, Abell J and Meyer J R 2012 *Proc. SPIE* **8374** 83740H
[13] Weih R, Kamp M and Hofling S 2013 *Appl. Phys. Lett.* **102** 231123
[14] Yang R Q and Pei S S 1996 *J. Appl. Phys.* **79** 8197
[15] Canedy C L, Abell J, Merritt C D, Bewley W W, Kim C S, Kim M, Vurgaftman I and Meyer J R 2014 *Proc. SPIE* **9002** 90021C
[16] Xing J L, Zhang Y, Liao Y P, Wang J, Xiang W, Xu Y Q, Wang G W, Ren Z W and Niu Z C 2014 *Proc. SPIE* **9002** 90021C
[17] Bewley W W, Canedy C L, Kim C S, Kim M, Merritt C D, Abell J, Vurgaftman I and Meyer J R 2012 *Opt. Express* **20** 20894
[18] Bauer A, Dallner M, Kamp M, Hofling S, Worschech L and Forchel 2010 *Opt. Eng.* **49** 111117
[19] Vurgaftman I, Bewley W W, Merritt C D, Canedy C L, Kim C S, Abell J, Meyer J R and Kim M 2012 *Proc. SPIE* **8268** 82681F
[20] Meyer J R, Hoffman C A, Bartoli F J and Ram-Mohan L R 1995 *Appl. Phys. Lett.* **67** 757
[21] Vurgaftman I, Bewley W W, Canedy C L, Kim C S, Kim M, Merritt C D, Abell J, Lindle J R and Meyer J R 2011 *Nat. Commun.* **2** 585